Bulletin of Engineering Geology and the Environment

Weak foliated rock slope stability analysis with ultra-close range terrestrial digital photogrammetry

--Manuscript Draft--

Manuscript Number:	BOEG-D-17-00276R1
Full Title:	Weak foliated rock slope stability analysis with ultra-close range terrestrial digital photogrammetry
Article Type:	Original Article
Corresponding Author:	Pedro Alameda-Hernández, Ph.D. Federal University of Ouro Preto OURO PRETO, Minas Gerais BRAZIL
Corresponding Author Secondary Information:	
Corresponding Author's Institution:	Federal University of Ouro Preto
Corresponding Author's Secondary Institution:	
First Author:	Pedro Alameda-Hernández, Ph.D.
First Author Secondary Information:	
Order of Authors:	Pedro Alameda-Hernández, Ph.D.
	Rachid El Hamdouni
	Clemente Irigaray
	José Chacón
Order of Authors Secondary Information:	
Funding Information:	Ministerio de Educación y Ciencia. Spanish government (CGL2008-04854/BTE) — Ph.D. Clemente Irigaray
Abstract:	This paper presents a review of the data acquisition procedures of geotechnical parameters for rock slope stability assessment and the proposal of some new improvements. For this purpose, a piece of research based on the Slope Mass Rating classification system using close range terrestrial digital photogrammetry (CR-TDP) has led to improvements in quality and timing of discontinuity data acquisition and analyzes the suitability of each one of the parameters when applied to weak foliated rocks. TDP allows rapid 3D image acquisition of a rock slope, which can be analyzed using software to determine the geometrical parameters that affect stability. A fast procedure to perform the photogrammetric, non-contact survey in order to obtain the 3D images is shown in this paper. Being rapid and single person, this procedure provides enough precision to be applied to weak foliated rock slopes with non-well defined geometry. Furthermore, the study has focused on highly foliated rock outcrops, in which the high resolution in the 3D images is very desirable. This research was applied to mountain road cuts, in which the use of TDP with a very close range was necessary, in one case of only four meters. Through an application on weak rocks in the Alpujarras (Andalusia, Spain), this work analyzes the bias when applying TDP to materials such as these, under progressive weathering processes.

1. Introduction

Rock slope stability estimation depends on the acquisition of a large quantity of outcrop data and on the method chosen to compute these data. Different surveying techniques shall lead to different values for the parameters on the same slope; furthermore, the same reasoning can be used with the parametrization system and with the computation method. A rock outcrop survey is laborious, time consuming and often expensive, as well as being generally biased. These considerations show the need for an automatized, less arduous, and faster surveying technique together with a standardized parametrization system.

This paper applies classification systems for the estimation of rock slopes stability, which will determine the parameters to be obtained. Regarding the classification systems, since Terzaghi (1946), many authors have presented other proposals for rock slope stability assessment using classification systems. A general overview can be found in Singh and Goel (1999) and Pantelidis (2009) while the recommended procedures from the International Society of Rock Mechanics can be found in Ulusay and Hudson (2007). However, the most widely used rock mass classification systems are Rock Mass Rating (RMR) (Bienawski 1973, 1989), Q (Barton et al. 1974) and Geological Strength Index (Hoek 1994; Hoek et al. 1998). The two first are specially indicated for underground works, being more limited for slopes, while Slope Mass Rating (SMR) (Romana 1985) offers higher reliability (Moon et al. 2001). SMR is a classification system partially based on RMR which is at the same time based on the Rock Quality Designation index (RQD) (Deere 1963).

The calculation of RQD was originally defined for its assessment on drilling samples. However, obtaining them is expensive, time consuming and laborious. Moreover, this calculation encompasses a bias because of the borehole orientation and length, and the need of a threshold value (Harrison 1999; Choi and Park 2004; Palmström 2005). Furthermore, RQD is not adequate for foliated rock massifs or for undisturbed ones, where it might adopt the highest (100%) or the lowest value (0%) in a wide variety of rock massifs. Besides, RQD can be estimated by means of scanlines (Priest and Hudson 1976; Olivier 1976; Sen and Kazi 1984; Palmström 2005), avoiding the need of boreholes, but with the same bias drawback. This paper applies Palmström (1974) and Priest and Hudson (1976) approaches.

Apart from the development of new classification systems, improvements and additions have been proposed by several authors for the already existing systems (e.g.; Marinos and Hoek 2000; Palmström and Broch 2005; Tomás et al. 2007). The aim of the new proposals is to determine better theoretical models for rock masses, with higher reliability and smaller sampling bias. However, despite these improvements, working with considerable uncertainty in rock mass stability analysis is still necessary.

The classical, direct-contact, surveying techniques for determining rock slope mechanical data (Ulusay and Hudson 2007) are especially laborious, time-consuming and sometimes dangerous because the rock outcrop might be not accessible for direct-contact sampling; hence, leading to the increasing use of remote sensing acquisition techniques. The main techniques for geomechanical characterization are terrestrial digital photogrammetry (TDP) and laser scanner (LS) (Ferrero et al. 2011), which are specially suitable for tunnels (Cacciari 2016, Menéndez-Diaz 2016). Furthermore, other RADAR based approaches (Osasan and Afeni 2010) are usually utilized for slope monitoring, especially satellite based for open-pit-mining operations. These techniques provide 3D point clouds or even terrestrial digital models to be analyzed in office in order to determine the slope and discontinuities orientation, visible size and position. Data acquisition from point clouds can be as meticulous as needed according to the analysis procedure while the classical direct-contact methods requires all data acquisition in field before the analysis, which can be a time-consuming arduous process.

When compared with LS, the TDP equipment is more affordable and easier to handle (Haneberg 2008); the main expense involved consists of a digital single lens reflex (DSLR) camera and a commercial software license. Due to the availability of commercial software, the image processing is fast, and their results are reliable (Sturzenegger and Stead 2009; Gaich et al. 2006; Krosley and Schaffner 2003).

TDP allows rapid remote data acquisition of geometrical data with millimeter accuracy (Sturzenegger and Stead 2009) at long distances (Sturzenegger et al. 2009; Pate and Haneberg 2011). Those applications are under strong development; images can be taken from a helicopter (Salvini et al. 2011), boat (De vita et al. 2012), with a reamed bar or an aerostatic balloon (Firpo et al. 2011; Salvini 2013) and even with unmanned aerial vehicles (Francioni 2015). Furthermore, it has been applied for studying joint roughness (Haneberg 2006; Kim et al. 2013; Aguilar et al. 2009). Spacing, persistence and RQD can be automatically derived from 3D point clouds as shown in Riquelme et al. (2015) and in Table 1 from Riquelme et al (2016). Aside from engineering geology, TDP has been applied for restoration works of artistic painting or sculpture surfaces (Bracci et al. 2013; Rescic et al. 2012; Barbetti et al. 2013).

However, conventional TDP, based on two images, has the inconvenience of producing more shadows than the LS technique (Roncella et al. 2005); however Structure from Motion (SfM) photogrammetric techniques avoid this inconvenience by using many photos from different points of view (Duelis Viana et al. 2016; Niederheiser et al. 2016; Chesley et al. 2017). SfM can utilize consumer cameras for a subsequent dense image matching (James and Robson 2012; Remondino et al. 2014).

When compared with the classical manual method, vegetation and infilling material within the outcrop surface might occlude some parts of it. Furthermore, when a rock slope presents a discontinuity set originated due to foliation, and this foliation is approximately parallel to the slope surface, the slope shows a stepped shape. Hence, discontinuities orientation is calculated by measuring step surfaces. However, the orientation of those steps surfaces can be altered due to weathering, making them more parallel to the slope and increasing their dip. This paper shows this phenomenon, which must be taken into account, especially because this discontinuity set might wrongly be assumed to be a cause of planar failure.

Two different data acquisition procedures have been applied in this paper: the traditional direct-contact method with compass, clinometer and measuring tape carried out directly on each rock slope and the photogrammetric one with the help of the commercial software SIROVISION (developed by CSIRO Mining and Exploration Division in Brisbane, Australia). Aside, DIPS V6 (ROCSCIENCE in Toronto, Ontario, Canada) has been applied for stereographic projection and kinematic analysis (Irigaray et al. 2012).

Apart from Sirovision (Haneberg 2006; 2008; Pate and Haneberg 2011), there are other commercial software for similar purposes. 3DM Analyst (Adam Technologies, from Perth, Australia) (Birch 2006; Wolter et al. 2014) and ShapeMetriX for point cloud acquisition together with JointMetriX for geometrical analysis (3GSM Software and Measurement, from Graz, Austria) (Gaich et al. 2006; Buyer and Shubert 2016). Furthermore, some researchers have developed their own software tools such as RockScan (Ferrero et al. 2009) for geometrical analysis, Virtuozzo (Roncella et al. 2005) for point cloud acquisition and DSE (discontinuities set extractor), an open access software offered by Riquelme et al. (2014). Other general-purpose photogrammetric software can be used in the rock slope 3D point clouds acquisition, an overview can be found in Niederheiser et al. (2016).

The conventional close range TDP methodology used in this paper is faster than the other procedures shown in the technical literature. This methodology provides good results even in rock slopes with a non-well defined geometry due to weathering in weak materials. Another aim of this research is to show the sampling bias when surveying on weak foliated rock slopes through TDP. All these results are derived from de determination of SMR parameters on road rock slopes in the Alpujarras of Granada province (Spain), showing, furthermore, an SMR limitation for this lithology regarding the low influence of roughness in its final rating.

2 Study area

The slopes studied are cuts along the A-348 Alpujarras road belonging to the Alcázar unit (Alpujárride Complex, Aldaya 1979), which is mainly composed of Permian and Lower Triassic weak foliated rocks (Fig. 1). This road, which is 146 km in length, is the only route that crosses a mountainous area populated by small scattered settlements, and has presented frequent rock slopes instability problems associated to heavy rainfalls and snow episodes. Two data sampling stations were analyzed:

Slope 1 (T1), kilometric point (k.p.) 33.000, is composed of mica schist bearing veins of quartz up to 4 cm wide (Fig. 2), slightly weathered and already affected by several shallow rockslides.

Slope 2 (T2), k.p. 33.200, (Fig. 3), is divided into two homogeneous zones according to the discontinuity orientations (T2a and T2b). It is composed of a set of strongly foliated mica schist (Alcántara-Ayala 1999) moderate to highly weathered. Besides the intense penetrative foliation, the rock massif is highly jointed and shows substantial heterogeneity due to the deformation produced by tectonic movements.

Fig. 1 Geographical setting of the analyzed rock outcrops analyzed

Fig. 2 T1 slope material; a mica schist showing a) a stepped surface b) quartz veins

Fig. 3 T2 slope material. Strongly foliated mica schist

3 Methods

3.1 Classification systems applied

For the purposes of this research the SMR (Romana 1985) has been chosen. Therefore, the SMR parameters (F_1, F_2, F_3, F_4) have been calculated along with the RMR_i parameters (V_1, V_2, V_3, V_4, V_5). Moreover, V_2 has been adjusted to the RQD. Finally, $SMR=(V_1+V_2+V_3+V_4+V_5)+(F_1 \cdot F_2 \cdot F_3)+F_4$ (1).

Most of these parameters were originally defined as distinct variables. Nonetheless in this work continuous variables have been applied as proposed by Romana (1997), Irigaray et al. (2003) and Tomás et al. (2007):

$$V_1 = \begin{cases} 1 + 0.1 \cdot UCS, & UCS < 40 \\ 0.1 \cdot UCS, & UCS \geq 40 \end{cases} \quad (2)$$

$$V_2 = \begin{cases} 3 + 0.1 \cdot RQD, & RQD \leq 20 \\ 2 + 0.15 \cdot RQD, & 20 \leq RQD \leq 40 \\ 0.2 \cdot RQD, & RQD \geq 40 \end{cases} \quad (3)$$

$$V_3 = \begin{cases} -5.16667 \cdot 10^{-6} \cdot s^2 + 0.0145667 \cdot s, & s < 1000 \\ 0.0056 \cdot s + 8.8, & 1000 < s < 2000 \end{cases} \quad (4)$$

Where *s* is the spacing between discontinuities in mm, and UCS the Uniaxial Compressive Strength in MPa.

Furthermore, V_4 and V_5 depend on joints condition and water presence, respectively. Thus, RMR_i value has been calculated following the guidance of Bieniawski (1989) with the addition of Eqs. (2)-(4).

Regarding the calculation of the final SMR and according to Tomás et al. (2007):

$$F_1 = (1 - |\sin(\alpha - \alpha_s)|)^2 \quad (5)$$

With α_s the slope direction and $\alpha=\alpha_j$ (α_j discontinuity dip direction) for plane failure (p) and toppling (t) and $\alpha=\alpha_i$ (the trend of the intersection line between two sets) for wedge failure (w).

$$F_2 = \begin{cases} \tan^2\beta\,, & \beta < 45º \\ 1, & \beta \geq 45º \end{cases} \quad (6)$$

With $\beta=\beta_j$ (set dip) for p, $\beta=\beta_i$ (trend of the intersection line between two sets) for w and $F_2=1$ for t.

Finally, according to Tomás et al. (2007):

$$F_3 = \begin{cases} -30 + \frac{1}{3}\cdot \mathrm{atan}(\beta_j - \beta_s)\,, (p) \\ -30 + \frac{1}{3}\cdot \mathrm{atan}(\beta_i - \beta_s),\ (w) \\ -13 - \frac{1}{7}\cdot \mathrm{atan}(\beta_j + \beta_s - 120),\ (t) \end{cases} \quad (7)$$

Being β_s the slope dip.

According to Priest and Hudson (1976) $RQD=100\cdot\exp(-t\cdot\lambda)\cdot(t\cdot\lambda+1)$ (8). Most commonly, t=0.1 m, as has always been set in this research. λ has been determined as the number of discontinuities that would appear per meter in a theoretical borehole as shown in Fig. 4. This borehole was considered perpendicular to the discontinuity family representing the schistosity, which was identified as the main cause of instability. The equation applied is: $\lambda = \sum 1/(s_i/\cos(a_i))$ (9), where s_i is the spacing for each discontinuity family (in meters) and a_i the minimum angle between the theoretical borehole and the line perpendicular to the discontinuity.

Furthermore, this paper applies the Volumetric Joint Count (J_v) (Palmström 1974) $RQD=115-3.3\cdot J_v$ (10). However, there is a poor correlation between J_v and RQD (Palmström 2005) and it would be more advisable to apply directly J_v with the Block Volume (V_b). Following the discussion section reasoning, the RQD value that has finally been chosen is Eq. (8).

Fig. 4 Frequency (λ) theoretical estimation for Eq. 7. In this example would be 6 (pieces of intact core, dimensionless) divided per the cube height (m)

3.2 Kinematic analysis

SMR refers to each specific kind of failure, thus it includes the slope and discontinuities geometrical attitude, hence, the kinematic analysis might be considered redundant. However, it has been performed as a previous step in order to visualize the kinematic compatibility and for a further validation of the SMR approach.

The non-geometrical information included in the kinematic analysis is the friction angle for the discontinuity surface (Φ). The only discontinuity set which Φ value has been applied in this paper calculi is the one developed through the foliation planes in both rock masses studied. Φ was set equal to the basic friction angle (Φ_b), which is a conservative approach but already applied (Admassu and Shakoor 2013) and reasonable because the rock mass is weak, this discontinuity set has been developed with a low spacing value and the joint surfaces are planar, smooth and even slickenside for T2. Barton and Choubey (1977) offered a Φ_b values summary for different lithologies, which has been consulted in this research. Consequently, the values chosen were Φ=26º for T1 and Φ=22º T2.

3.3 Data acquisition

This research uses TDP for analyzing mountain road cut rock slopes, where the horizontal surface adjacent to them might be as narrow as less than 10 m wide, which means the camera must be placed at a very short distance from the object (Thoeni et al. 2014; Kim et al. 2016). Furthermore, the type of rock studied requires high resolution because of its foliation. Point clouds have been successfully obtained by a single person photogrammetric survey without the use of a GPS or theodolite, only using a measuring tape, a tripod and a compass.

Fig. 5 Rock slope stability analysis flowchart.

Therefore, the procedure followed in this work consists of measuring the slope orientation (α) with a compass, setting the camera horizontally at the desired distance (range, S) and orienting it perpendicularly to the slope by using the tripod bubble level and the compass. This camera position is called C1 in Fig. 6. The following step consists of identifying the central point of the image with that camera position by looking through the camera, this shall be the control point (CP) (Fig. 6), therefore it must be marked with spray, chalk or similar. Finally, the camera is located on the second point (C2) for taking the second image, again horizontally and with the same height as in C1. For this purpose, the distance among C1 and C2 (base, b) must be set around 1/8 S and 1/6 S according to CSIRO instructions.

Fig. 6 TDP data acquisition. PC: ground control point. C1, C2: Camera positions. B': Survey matrix for local axis. *S*: range. *b*: base

Thus, this method needs two images along with three numerical data (*b*, *S* and α). The point cloud can be mounted with b and S in local axis. Finally, it will be oriented with α consequently obtaining a 3D model vertical and north-oriented. If desired, a GPS survey point could be used for obtaining absolute coordinates.

The photographic equipment used in this work was a Canon EOS 40D single lens reflex (SLR) camera with a 22.2x14.8 mm CMOS sensor and 10.10 effective Mpix. The lenses had focal lengths of 24 and 50 mm (Table 1).

Table 1 Photographs parameters. S: range. b: base. f: focal length. W: width. H: height.

Slope	*S* (m)	*b* (m)	f (mm)	Size (WxH m) (aprox.)
T1	17.8	2.2	50	3.9x3.2
T2a	6.5	1	24	5.2x2.2
T2b	6.6	1	24	4.9x2.1

Because of the good illumination during the field work, ISO speed was set to the lowest value (ISO-100), with the optimum aperture, F8, and the time of exposure was never above 1/100 s.

Another direct-contact survey for validating the photogrammetric procedure was carried out in this work. It took around 3 hours whereas the TDP fieldwork took 20 minutes.

After obtaining the point cloud, Sirovision software offers a tool for automatic joints recognition; an alternative MATLAB code with a similar tool for semiautomatically extracting discontinuity sets has been developed by Riquelme et al. (2014). However, in this research the discontinuity surfaces cropping out had not enough size to be identified automatically. Hence, joint identification was performed on the point cloud display by tracing them with the cursor.

Hence, in this work, spacing values were assessed by measuring the distance between discontinuity traces along a scanline in the point cloud surface and multiplying it by the sine of the angle between the lower discontinuity and the slope face.

4 Results and discussion

4.1 Geometry

The point clouds showed rotation regarding the real orientation measured with the direct-contact method. This rotation, 10º, 21º and 5º respectively for T1, T2a and T2b slopes is due to the fact that only one control point was taken into account and neither a theodolite nor a GPS was used. However, this rotation is not a considerable drawback; it was easily identified and corrected using DIPS software. Furthermore, the discontinuities were projected and sets were identified, which can be seen in Fig. 7 for slope T2a: S0, drawn in red, comes from schistosity, J1, in blue and J2 in green are both joint sets. Table 2 summarizes this information for all the slopes.

Table 2 Dip/dip direction

SLOPE		S_0		J_1		J_2	
		TDP	Direct-contact	TDP	Direct-contact	TDP	Direct-contact
T1	60º/80º	24º/91º	14º/130º	82º/320º	73º/319º	54º/230º	52º/231º
T2a	85º/100º	22º/151º	27º/160º	63º/329º	58º/328º	38º/230º	26º/239º
T2b	85º/80º	19º/128º	23º/143º	68º/328º	69º/316º	30º/202º	30º/228º

Fig. 7 T2a slope kinematic analysis. a) With direct-contact survey data b) With photogrammetric survey data

4.2 Kinematic analysis

Despite no pure kinematic compatibility with failure was found, SMR was calculated in slope T2a for plane failure through S_0 and wedge through S_0-J_1 and S_0-J_2 for all slopes because the kinematic analysis was very close to show compatibility in those cases (Figs. 8 and 9), and considering that kinematic stereonet-based method might have a lack of reliability because of not considering correctly the wide variability in discontinuity data (Admassu and Shakoor 2013), specially for wedge failure, where the number of potential discontinuity intersections is enormous (Fig 8c).

Fig. 8 T2b slope. a) Discontinuities and sets, represented trough poles and slope and mean set planes b) Plane failure: no kinematic compatibility (red area regards set poles) c) Wedge. No kinematic compatibility but close by means of S_0-J_1 and S_0-J_2

Fig. 9 T1 slope. Kinematic analysis (P) through discontinuity poles, for: a) direct-contact data and b) TDP data

4.3 RMR_i parameters

V_1 depends on the intact rock UCS (Eq. 2). The Schmidt Hammer, or sclerometer, (Miller 1965) offered very low values when applied perpendicularly to schistosity planes and very high ones when applied in the parallel direction (Table 3). Thus, for the estimation of UCS, the columns on the right of Table 3 were used.

Table 3. UCS estimation. R: rebound measured by the Schmidt Hammer (which units follow an arbitrary scale)

Slope	R (units)	γ (g/cm^3)	UCS (from R)	Field identification	UCS (ISRM, 1978)	V_1
T1	50	2.8	≥120 MPa	Rock can be laminated by firm blow with point of geological hammer.	**20 MPa**	**1.2**
T2	36	2.7	≈65 MPa	Rock can be peeled with a pocket knife.	**10 MPa**	**1.1**

V_2 (Eq. 3) depends on RQD Eqs. (8)-(10) (Table 4).

Table 4. RQD estimation

	s_m (m)			λ (m^{-1})	J_v (m^{-3})	RQD^a (Eq. 8)	RQD^b (Eq. 10)
SLOPE	S_0	J_1	J_2				
T1	0.076	0.086	0.11	18.7	33.88	44.2%	3.2%
$T2_a$	0.11	0.20	0.20	12.3	19.09	65.1%	52.0%
$T2_b$	0.08	0.30	0.18	17.1	21.39	49.0%	44.4%

Palmström (1974) equation offers an RQDb value which seems to be excessively low for slope T1 whereas RQDb behaves more consistently. Furthermore, Priest and Hudson (1976) equation (8) considers the borehole orientation, which in this situation is desired to be perpendicular to the schistosity set; this has been applied in these calculi. Thus, V_2 values according to RQDa results 8.8, 13 and 9.8 for T1, T2a and T2b, respectively. λ was calculated with Eq. 9 considering the orientation values from the direct-contact survey shown in Table 2, which lead us to the values shown in Table 5.

Table 5. a_i values (minimum angle among the theoretical borehole and the perpendicular line to the family)

	T1			T2$_a$			T2$_b$		
	S_0	J_1	J_2	S_0	J_1	J_2	S_0	J_1	J_2
a_i(º)	0	87	57	0	86	55	0	88	36

V_3 (Eq. 4) has been calculated for each discontinuity family, as shown in Table 6.

Table 6. V_3 values

	T1			T2$_a$			T2$_b$		
	S_0	J_1	J_2	S_0	J_1	J_2	S_0	J_1	J_2
s(m)	0.076	0.086	0.11	0.11	0.20	0.20	0.08	0.30	0.18
V_3	**6.1**	**6.2**	**6.6**	**6.6**	**7.9**	**7.9**	**6.2**	**9.4**	**7.6**

V_4 consists of a set of visual estimations ($V_{4,3}$, $V_{4,4}$, $V_{4,5}$) and field measurements ($V_{4,1}$, $V_{4,2}$) (Table 7)

Table 7. V_4 through its subparameters

	T1			T2a			T2b		
	S_0	J_1	J_2	S_0	J_1	J_2	S_0	J_1	J_2
P (cm)	52	38	72	47	24	36	54	50	50
$V_{4,1}$	6	6	6	6	6	6	6	6	6
Ap (mm)	None	1	<1	<1	3	<1	<1	2	<1
$V_{4,2}$	6	1	5	5	1	5	5	1	5
Ro	SM	R	SM	SS	SR	SM	SS	SR	SM
$V_{4,3}$	1	4	2	0	3	2	0	3	2
In	N	S	N	N	S	H	N	S	H
$V_{4,4}$	6	2	6	6	2	5	6	2	5
W	MW	MW	SL	HW	MW	MW	HW	MW	MW
$V_{4,5}$	2	3	4	1	2	3	1	2	3
V_4	21	16	23	18	14	21	18	14	21

P: Persistence, Ap: Aperture, Ro: Roughness, In: Infilling, W: Weathering

SS: Slickenside, SM: Smooth, SR: Slightly rough, R: Rough

N: None, S: Sandy, loose, H: Hard

SL: Slightly weathered, MW: Moderately weathered, HW: Highly Weathered

$V_4=V_{4,1}+ V_{4,2}+ V_{4,3}+ V_{4,4}$

$V_{4,1}$ considers all the traces below 1m length as equal. Materials in this research offer a non-well-structured geometry and discontinuities show low persistence. Thus, RMR_i assigns the same $V_{4,1}$ value for all these materials despite the differences among them.

$V_{4,3}$ depends on a visual estimation of rock surface roughness although there are many methods for quantifying it (Tse and Cruden 1979; Kulatilake et al. 1995; Tatone and Grasselli 2010; Alameda-Hernández et al. 2014). Furthermore, it only represents 6 over 95 RMRi possible punctuation, however roughness might be an important parameter for foliated materials when schistosity gives place to a discontinuity familiy kinematically compatible with plane failure.

No moisture was observed during field research, thus V_5 took its highest value. The resulting RMR_i values are shown on Table 8.

Table 8. RMR_i values

	T1			$T2_a$			$T2_b$		
	S_0	J_1	J_2	S_0	J_1	J_2	S_0	J_1	J_2
RMRi	52.1	47.2	54.6	53.7	51	58	50.1	49.3	54.5

4.4 SMR parameters

F_1, F_2 and F_3 are automatically calculated by Eqs. (5)-(7) from the discontinuity families and slopes orientation values (Table 8).

Table 9. T1 SMR parameters

Fail.		S_0 (P)		S_0-J_1 (W)		S_0-J_2 (W)	
Sur.		Direct	TDP	Direct	TDP	Direct	TDP
T1	Or.	14º/130º	24º/91º	48º/2º	47º/17º	151º/14º	149º/13º
	F_1	N. C.	0.655	0.221	0.207	0.003	0.004
	F_2		0.2	0.001	0.093	0.06	0.05
	F_3		-59.47	-59.67	-59.56	-59.58	-59.59
	F_1. F_2. F_3		**-7.79**	**-0.01**	**-1.15**	**-0.01**	**-0.01**
T2a	Or.	27º/160º	22º/151º	240º/4º	239º/1º	200º/22º	169º/21º
	F_1	0.018	0.05	0.128		≈0	0.004
	F_2	0.260	0.163	0.005	≈0		0.147
	F_3	-59.67	-59.7	-59.76			-59.7
	F_1. F_2. F_3	**-0.28**	**-0.49**	**-0.04**	**≈0**	**≈0**	**-0.03**
T2b	Or.	23º/143º	19º/128º	227º/3º	55º/5º	174º/20º	147º/18º
	F_1	N. C.	0.066	0.207	0.333	≈0	0.006
	F_2		0.119	0.003	0.008		0.105
	F_3		-59.71	-59.77	-59.76		-59.72
	F_1. F_2. F_3		**-0.46**	**-0.04**	**-0.16**	**≈0**	**-0.04**

Fail: Failure mechanism: P: Planar. W: Wedge. N. C: Not compatible

Sur: Survey method: Direct: Direct-contact. TDP: Photogrammetric

Or: Orientation: Dip/Dip Direction for planes. Trend/Plunge for intersections

The mechanical excavation in both slopes makes F_4=0. Thus, by modifying RMR_i with the four SMR parameters, the obtained final SMR value is shown in Table 10. All slopes are class III, thus fair and partially stable, but they would need some reinforcements, like bolts or anchors, especially for slope T1, according to the Romana (1983; 1993) guidelines.

Table 10. SMR according to the most unfavorable failure mechanism (fail. mech.)

	T1	Fail. mech.	T2a	Fail. mech.	T2b	Fail. mech.
SMR (Direct)	50	Wedge S_0-J_1	52	Wedge S_0-J_1	50	Wedge S_0-J_1
SMR (TDP)	44	Planar S_0	52	Wedge S_0-J_1	50	Wedge S_0-J_1
Direct: Direct-contact survey. TDP: photogrammetric survey						

4.5 Bias due to weathering in weak rocks in a photogrammetric survey

A discontinuity orientation can be measured through a plane or through a trace. During a direct-contact survey this can be done by directly placing the compass over a piece of plane or over a trace with the help of a folder or any other similar item. TDP allows automatic measuring using either a plane or a trace.

Weathering over surfaces belonging to a set quite parallel to the slope and with less inclination shall make the set seem more parallel and inclined (Fig. 10).

During a direct-contact survey, the evaluator can estimate the weathering effect and correct it when measuring through a plane. This correction is not automatically performed by the software, however, measurements can be taken through traces, which are not affected by this; traces offer the real discontinuity orientation. This bias can be seen in the discontinuity sets developed by the schistosity, S_0. Table 11 shows results with direct-contact methods where the evaluator took the weathering into account, and the photogrammetric survey from both traces and planes. Furthermore, this can be seen in Fig. 11, which shows measurements taken through planes more inclined and parallel to the slope.

Table 11. Dip/Dip direction for set S_0

Slope	Slope Dip Direction	Direct-contact	TDP (Traces)	TDP (Planes)
T1	80°	14°/130°	21°/97°	25°/90°
T2a	100°	27°/160°	21°/179°	26°/134°
T2b	80°	23°/143°	19°/160°	21°/111°

Fig. 10 T2a slope. Weathering effect when measuring S_0 orientation with TDP through a plane a) No weathering (A) b) Weathered surfaces (B) c) A "step" in the slope

Fig. 11 T2a slope. S_0 set representation by means of both direct-contact and TDP survey. Further comparison among TDP values obtained through planes and through traces

5 Conclusions

SMR classification system should be adapted for being applied to foliated weak rocks, because, despite being considered as suitable for them (Moon et al. 2001), it has some drawbacks when applied to these rocks, especially because it depends on RMRi. Apart from other well-known considerations, such as the lack of appropriateness of the Rock Quality Designation or Unconfined Compressive Strength for these lithologies, this paper highlights that:

- Roughness is an important parameter regarding foliated rock slope stability, especially regarding plane failure through a discontinuity family developed because of the foliation. However, it is not of considerable importance in this classification system.
- The RMRi parameter regarding persistence has no proper intervals for these rocks. It classifies a wide variety of rock massifs equally because the lowest interval encompasses traces up to 1 m in length.

Regarding Terrestrial Digital Photogrammetry; TDP can be applied to foliated weak rock slopes with non-well defined geometry:

- Furthermore, there is no need of utilizing GPS or any expensive equipment. A rapid, single person fieldwork procedure using a tripod with a bubble level, a measuring tape and a compass provides enough precision.
- Weathering must be considered in photogrammetric surveys. If a discontinuity family is approximately parallel to the slope and has a higher dip, it will seem to be more inclined and more parallel to the slope due to weathering. This can be directly avoided if point cloud measurements are taken on discontinuities traces, not on discontinuities surfaces.

The incessant and rapid current technological development is providing rock mechanics with new powerful data acquisition tools that must be applied with a research attitude in order to be tested and validated, discovering their capabilities as well as their limitations. Furthermore, automated comprehensive rock mass stability analysis procedures must be arranged for each one of these new data acquisition techniques, for each lithology or group of lithologies; with that focus this paper presents a comprehensive procedure for weak foliated rock slope stability analysis including a rapid, single person and economical conventional Terrestrial Digital Photogrammetry technique.

References

Admassu Y, Shakoor A (2013) Cut slope design recommendations for sub-horizontal sedimentary rock units in Ohio, USA. Geotechnical and Geological Engineering, 31 (4):1207-1219. DOI: 10.1007/s10706-013-9644-4

Aguilar MA, Aguilar FJ, Negreiros J (2009) Off-the-shelf laser scanning and close-range digital photogrammetry for measuring agricultural soils. Biosystems Engineering, 103:504-517. DOI: http://dx.doi.org/10.1016/j.biosystemseng.2009.02.010

Alameda-Hernández P, Jiménez-Perálvarez J, Palenzuela JA, El Hamdouni R, Irigaray C, Cabrerizo MA, Chacón J (2014) Improvement of the JRC calculation using different parameters obtained through a new survey method applied to rock discontinuities. Rock Mechanics and Rock Engineering 47 (6):2047-2060. doi: 10.1007/s00603-013-0532-2

Alcántara-Ayala I (1999) The Torvizcón, Spain, landslide of February 1996: the role of lithology in a semi-arid climate. Geofísica Internacional, 38

Aldaya F (1979) Mapa Geológico De España, Escala 1:50.000. IGME, Madrid (Spain)

Barbetti I, Felici A, Magrini D, Manganelli del Fa R Riminesi C (2013) Ultra close-range photogrammetry to assess the roughness of the wall painting surfaces after cleaning treatments. International Journal of Conservation Science 4:525-534.

Barton N, Choubey V (1977) The shear strength of rock joints in theory and practice. Rock Mechanics and Rock Engineering 10:1-54

Barton N, Lien R and Lunde J. (1974) Engineering classification of rock masses for the design of tunnel support. Rock Mechanics and Rock Engineering 6:189-236

Bhasin R, Barton N, Grimstad E, Chryssanthakis P (1995) Engineering geological characterization of low strength anisotropic rocks in the Himalayan region for assessment of tunnel support. Engineering Geology 40:169–193. DOI: 10.1016/0013-7952(95)00055-0

Bieniawski ZT (1973) Engineering Classification of Jointed Rock Masses. The Civil Engineer in South Africa 15:335-344

Bieniawski ZT (1989) Engineering rock mass classifications: a complete manual for engineers and geologists in mining, civil, and petroleum engineering. Wiley & Sons, New York (U.S.A.)

Birch JS (2006) Using 3DM Analyst Mine Mapping Suite for Rock Face Characterisation. Workshop: Laser and Photogrammetric Methods for Rock Face Characterization 13-32, Golden, Colorado (USA)

Bracci S, Cuzman OA, Ignesti A, Manganelli del Fa R, Olmi R, Pallecchi P, Riminesi C, Tiano P (2013) Multidisciplinary approach for the conservation of an etruscan hypogean monument. European Journal of Science and Theology 9(2):91-106

Cacciari PP, Futai MM (2016) Mapping and characterization of rock discontinuities in a tunnel using 3D terrestrial laser scanning. Bull Eng Geol Environ 75 (1): 223-237. doi:10.1007/s10064-015-0748-3

Chesley JT, Leier AL, White S, Torres R (2017) Using unmanned aerial vehicles and structure-from-motion photogrammetry to characterize sedimentary outcrops: An example from the Morrison Formation, Utah, USA. Sedimentary Geology 354(1): 1-8 ISSN 0037-0738, https://doi.org/10.1016/j.sedgeo.2017.03.013.

Choi SY, Park HD (2004) Variation of rock quality designation (RQD) with scanline orientation and length: a case study in Korea. International Journal of Rock Mechanics and Mining Sciences 41:207–221. DOI: 10.1016/S1365-1609(03)00091-1

De Vita P, Cevasco A, Cavallo C (2012) Detailed rock failure susceptibility mapping in steep rocky coasts by means of non-contact geostructural surveys: the case study of the Tigullio Gulf (Eastern Liguria, Northern Italy). Natural Hazards and Earth System Science 12:867-880. DOI: 10.5194/nhess-12-867-2012

Deere DU (1963) Technical description of rock cores for engineering purposes. Rock Mechanics and Engineering Geology 1

Duelis Viana C, Endlein A, da Cruz Campanha GA, Grohmann CH (2016) Algorithms for extraction of structural attitudes from 3D outcrop models. Computers & Geosciences 90 (Part A) 112-122, ISSN 0098-3004, https://doi.org/10.1016/j.cageo.2016.02.017

Ferrero A, Forlani G, Roncella R, Voyat H (2009) Advanced Geostructural Survey Methods Applied to Rock Mass Characterization. Rock Mechanics and Rock Engineering (42)631-665

Ferrero A, Migliazza M, Roncella R, Rabbi E (2011) Rock slopes risk assessment based on advanced geostructural survey techniques. Landslides 8:221-231

Firpo G, Salvini R, Francioni M, Ranjith PG (2011) Use of Digital Terrestrial Photogrammetry in rocky slope stability analysis by Distinct Elements Numerical Methods. International Journal of Rock

Mechanics and Mining Sciences 48:1045–1054. DOI: 10.1016/j.ijrmms.2011.07.007

Francioni M, Salvini R, Stead D, Giovannini R, Riccucci S, Vanneschi C, Gullì D (2015) An integrated remote sensing-GIS approach for the analysis of an open pit in the Carrara Marble District, Italy: slope stability assessment through kinematic and numerical methods. Comput Geotech 67:46-63. doi:10.1016/j.compgeo.2015.02.009

Gaich A, Pötsch M, Shubert W (2006) Basics and application of 3D imaging systems with conventional and high-resolution cameras. Laser and Photogrammetric Methods for Rock Face Characterization, Golden, Colorado (USA) 33-48.

Goshtasbi K, Ahmadi M, Seyedi J. (2006) Anisotropic strength behaviour of slates in the Sirjan-Sanandaj zone. The Journal of The South African Institute of Mining and Metallurgy 106:71-76

Haneberg WC (2006) 3-D rock mass characterization using terrestrial digital photogrammetry. AEG News 49:12-15

Haneberg WC (2008) Using close range terrestrial digital photogrammetry for 3-D rock slope modeling and discontinuity mapping in the United States. Bull Eng Geol Environ 67:457–469. doi:10.1007/s10064-008-0157-y

Harrison JP (1999) Selection of the threshold value in RQD assessments. International Journal of Rock Mechanics and Mining Sciences 36:673–685. DOI: 10.1016/S0148-9062(99)00035-2

Hoek E. (1994) Strength of rock and rock masses. ISRM News 2:4-16

Hoek E, Brown ET (1997) Practical estimates of rock mass strength. International Journal of Rock Mechanics and Mining Sciences 34:1165–1186. DOI: 10.1016/S1365-1609(97)80069-X

Hoek E, Marinos P, Benissi M (1998) Applicability of the geological strength index (GSI) classification for very weak and sheared rock masses. The case of the Athens Schist Formation. Bulletin of Engineering Geology and the Environment 57:151-160

Irigaray C, El Hamdouni R, Jiménez-Perálvarez JD, Fernández P and Chacón J (2012) Spatial stability of slope cuts in rock massifs using GIS technology and probabilistic analysis. Bulletin of Engineering Geology and the Environment 71:579-578

Irigaray C, Fernández T, Chacón J (2003) Preliminary Rock-Slope-Susceptibility Assessment Using GIS and the SMR Classification. Natural Hazards 30:309-324

ISRM (1978) International Society for Rock Mechanics commission on standardization of laboratory and field tests: Suggested methods for the quantitative description of discontinuities in rock masses. International Journal of Rock Mechanics and Mining Sciences & Geomechanics Abstracts 15:319–368. DOI: DOI: 10.1016/0148-9062(78)91472-9

James MR, Robson S (2012) Straightforward reconstruction of 3D surfaces and topography with a camera: Accuracy and geoscience application. Journal of Geophysical Research 117. doi:10.1029/2011JF002289

Kim DH, Gratchev I, Balasubramaniam A (2013) Determination of joint roughness coefficient (JRC) for slope stability analysis: a case study from the Gold Coast area, Australia. Landslides 10:657-664. DOI: 10.1007/s10346-013-0410-8

Kim DH, Poropat G, Gratchev I et al. (2016) Assessment of the Accuracy of Close Distance Photogrammetric JRC Data. Rock Mech Rock Eng 49 (11):4285-4301. doi:10.1007/s00603-016-1042-9

Krosley L, Schaffner P (2003) Applications and accuracy of photogrammetry for geological and geotechnical data collecting. Annal Meeting Abstracts, Vail, Colorado.

Kulatilake PHSW, Shou G, Huang TH, Morgan RM (1995) New peak shear strength criteria for anisotropic rock joints. International Journal of Rock Mechanics and Mining Science & Geomechanics

Abstracts 32:673–697. DOI: DOI: 10.1016/0148-9062(95)00022-9

Marinos P, Hoek E (2000) GSI: A Geologically friendly tool for rock mass strength estimation. GeoEng2000 Conference, Melbourne 1422-1442.

Menéndez-Díaz A, Argüelles-Fraga R, García-Cortés S et al. (2016) Stability analysis of a tunnel using LIDAR data and the keyblock method. Bull Eng Geol Environ 75 (2):469-483. doi:10.1007/s10064-015-0761-6

Miller RP (1965) Engineering classification and index properties for intact rock. PhD Thesis, Univ. of Illinois

Moon V, Russell G, Stewart M (2001) The value of rock mass classification systems for weak rock masses: a case example from Huntly, New Zealand. Engineering Geology 61:53–67. DOI: 10.1016/S0013-7952(01)00024-2

Niederheiser R, Mokros M, Lange J, Petschko H, Prasicek G, Elberink SO (2016) Deriving 3d point clouds from terrestrial photographs - comparison of different sensors and software. The International Archives of the Photogrammetry, Remote Sensing and Spatial Information Sciences (XXIII ISPRS Congress, 12–19 July 2016, Prague, Czech Republic). XLI(B5):685-692 doi:10.5194/isprsarchives-XLI-B5-685-2016

Olivier RJ (1976) Determination of RQD from petroscope obsevations. Expl. Rock Eng., Johannesborg, Balkema, Cape Town 63-68

Osasan K, Afeni T (2010) Review of surface mine slope monitoring techniques. Journal of Mining Science 46:177-186.

Palmström A (1974) Characterization of jointing density and the quality of rock masses. Internal report, A. B. Berdal, Norway

Palmström A (2005) Measurements of and correlations between block size and rock quality designation (RQD) Tunnelling and Underground Space Technology 20:362–377. DOI: 10.1016/j.tust.2005.01.005

Palmström A, Broch E (2005) Use and misuse of rock mass classification systems with particular reference to the Q-system. Tunnelling and Underground Space Technology 21:575–593. DOI: 10.1016/j.tust.2005.10.005

Pantelidis L. (2009). Rock slope stability assessment through rock mass classification systems. International Journal of Rock Mechanics and Mining Sciences 46:315–325. 10.1016/j.ijrmms.2008.06.003

Pate K, Haneberg WC (2011) Photogrammetric and LiDAR 3-D Rock Slope Discontinuity Mapping and Interpretation Surveys to Improve Baseline Information for Supporting Design and Construction of Capital Improvement Projects at Hydroelectric Facilities. 45th US Rock Mechanics / Geomechanics Symposium, San Francisco, CA (USA)

Priest SD, Hudson JA (1976) Discontinuity spacings in rock. International Journal of Rock Mechanics and Mining Sciences & Geomechanics Abstracts 13:135–148. DOI: 10.1016/0148-9062(76)90818-4

Remondino F, Spera MG, Nocerino E, Menna F, Nex F (2014) State of the art in high density image matching. The Photogrammetric Record 29: 144–166. doi:10.1111/phor.12063

Rescic S, Tiano P, Fratini F, Manganelli del Fà R (2012) The micro-sandblasting technique as a new tool for the evaluation of the state of conservation of natural stone and mortar surfaces. European Journal of Environmental and Civil Engineering 17(2):113-127. DOI: 10.1080/19648189.2012.751227

Riquelme AJ, Abellán A, Tomás R, Jaboyedoff M (2014) A new approach for semi-automatic rock mass joints recognition from 3D point clouds. Computers & Geosciences 68:38-52. http://dx.doi.org/10.1016/j.cageo.2014.03.014

Riquelme AJ, Abellán A, Tomás R (2015) Discontinuity spacing analysis in rock masses using 3D point clouds. Engineering Geology 195:185-195. doi: 10.1016/j.enggeo.2015.06.009

Riquelme AJ, Tomás R, Abellán A (2016) Characterization of rock slopes through slope mass rating using 3D point clouds. International Journal of Rock Mechanics and Mining Sciences, 84, 165-176, doi: http://dx.doi.org/10.1016/j.ijrmms.2015.12.008.

Romana M (1985) New adjustments ratings for application of Bieniawski classification to slopes. Int. Symp. on the Role of Rock Mechanics, Zacatecas 49-53.

Romana M (1993) A Geomechanical Classification for Slopes: Slope Mass Rating. In: John A. Hudson (ed) Comprehensive rock engineering. Imperial College. Pergamon Press, Oxford

Romana M (1997). El papel de las clasificaciones geomecánicas en el estudio de la estabilidad de taludes. IV Simposio Nacional Sobre Taludes Y Laderas Inestables, Granada, Spain 955-1011

Roncella R, Forlani G, Remondino F (2005) Photogrammetry for geological applications: automatic retrieval of discontinuity orientation in rock slopes. SPIE: Videometrics VIII, San Jose, California, USA, 17-27

Salvini R, Francioni M, (2013) Geomatics for slope stability and rock fall runout analysis: A case study along the alta tambura road in the apuan alps (Tuscany, Italy). Italian Journal of Engineering Geology and Environment 06 B-46:481-492. https://www.scopus.com/inward/record.uri?eid=2-s2.0-84888174843&doi=10.4408%2fIJEGE.2013-06.B-46&partnerID=40&md5=5502a21b9dd47048d1ac92bbfd9233e0",Article,Scopus,2-s2.0-84888174843

Salvini R, Francioni M, Riccucci S, Fantozzi P, Bonciani F, Mancini S (2011) Stability analysis of Grotta delle Felci Cliff (Capri Island, Italy): structural, engineering-geological, photogrammetric surveys and laser scanning. Bulletin of Engineering Geology and the Environment 70: 549-557

Sen Z, Kazi A (1984). Discontinuity spacing and RQD estimates from finite length scanlines. International Journal of Rock Mechanics and Mining Sciences & Geomechanics Abstracts 21:203–212. DOI: 10.1016/0148-9062(84)90797-6

Singh RK, Goel B (1999) Rock Mass Classification. A Practical Approach in Civil Engineering. Elsevier, Oxford (UK)

Sturzenegger M, Stead D (2009) Quantifying discontinuity orientation and persistence on high mountain rock slopes and large landslides using terrestrial remote sensing techniques. Natural Hazards and Earth System Science 9:267-287. DOI: 10.5194/nhess-9-267-2009

Sturzenegger M, Stead D, Beveridge A, Lee S, van As A (2009) Long-range terrestrial digital photogrammetry for discontinuity characterization at Palabora open-pit mine. CANUS Rock Mechanics Symposium, Toronto.

Tatone BSA, Grasselli G (2010). A new 2D discontinuity roughness parameter and its correlation with JRC. International Journal of Rock Mechanics and Mining Sciences 47:1391–1400. DOI: 10.1016/j.ijrmms.2010.06.006

Terzaghi K (1946) Rock Defects And Load On Tunnel Supports, Introduction To Rock Tunneling With Steel Supports. Commercial Shearing & Stamping Co., Youngstown, Ohio, U.S.A.

Thoeni K, Giacomini A, Murtagh R, Kniest E (2014) A comparison of multi-view 3D reconstruction of a rock wall using several cameras and a Laser scanner. International Archives of the Photogrammetry, Remote Sensing and Spatial Information Sciences – ISPRS Technical Commission V Symposium XL-5:573-580. https://www.scopus.com/inward/record.uri?eid=2-s2.0-84924275594&doi=10.5194%2fisprsarchives-XL-5-573-2014&partnerID=40&md5=03ca964df99b45865ebdb884ea348cf1

Tomás R, Delgado J, Serón JB (2007). Modification of slope mass rating (SMR) by continuous functions.

International Journal of Rock Mechanics and Mining Sciences 44:1062–1069. DOI: 10.1016/j.ijrmms.2007.02.004

Tse R, Cruden DM (1979) Estimating joint roughness coefficients. International Journal of Rock Mechanics and Mining Sciences & Geomechanics Abstracts 16:303–307. DOI: 10.1016/0148-9062(79)90241-9

Ulusay RH, Hudson JA (2007) The Complete ISRM Suggested Methods For Rock Characterisation, Testing And Monitoring: 1974-2006. Ulusay, R. Hudson, J. A. Ankara, Turkey

Wolter A, Stead D, Clague JJ (2014) A morphologic characterisation of the 1963 Vajont Slide, Italy, using long-range terrestrial photogrammetry. Geomorphology 206:147-164. DOI: http://dx.doi.org/10.1016/j.geomorph.2013.10.006

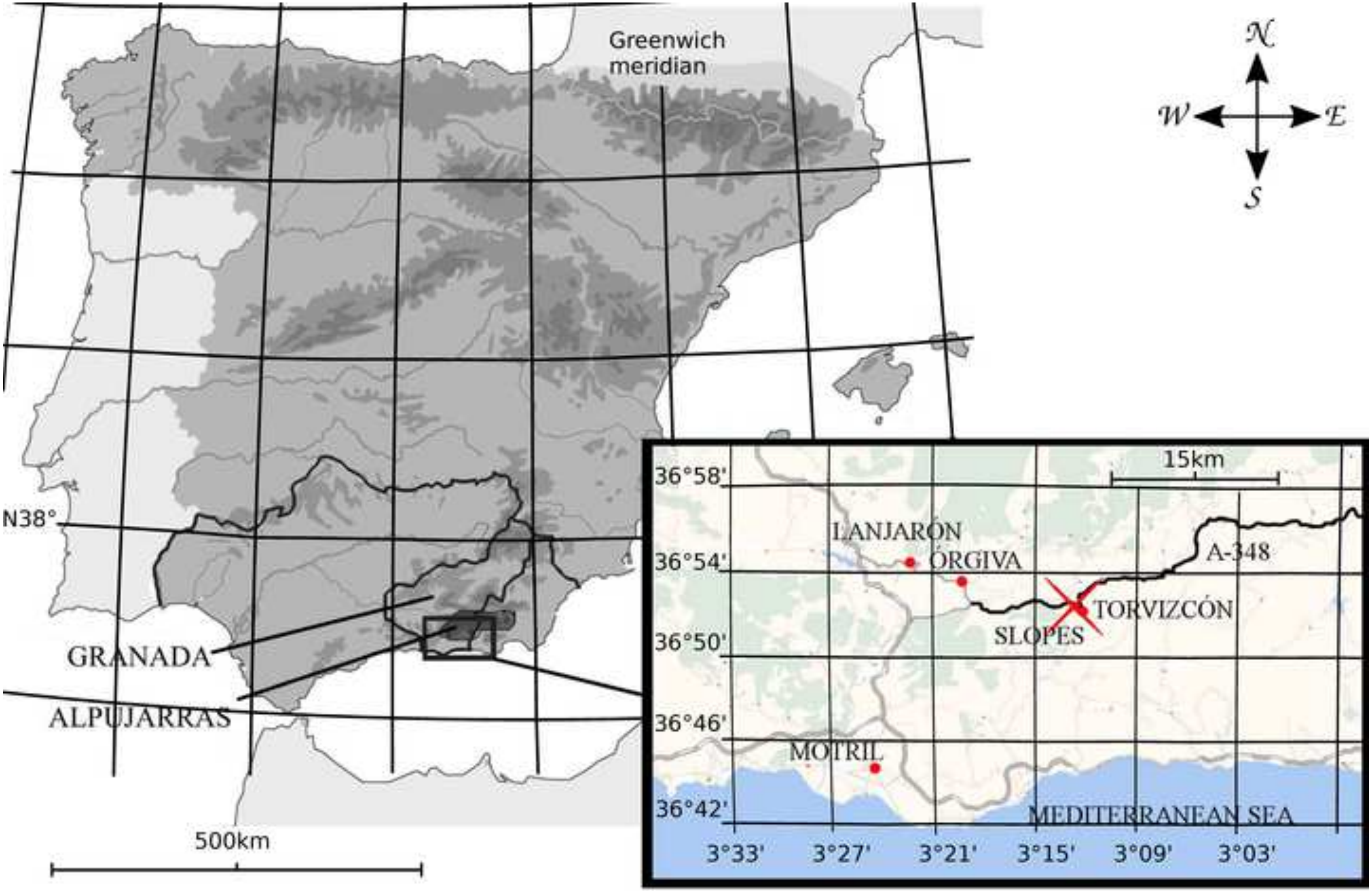
Greenwich meridian
N
W
E
S
N38°
GRANADA
ALPUJARRAS
500km
15km
36°58'
36°54'
36°50'
36°46'
36°42'
LANJARÓN
ÓRGIVA
A-348
TORVIZCÓN
SLOPES
MOTRIL
MEDITERRANEAN SEA
3°33'
3°27'
3°21'
3°15'
3°09'
3°03'

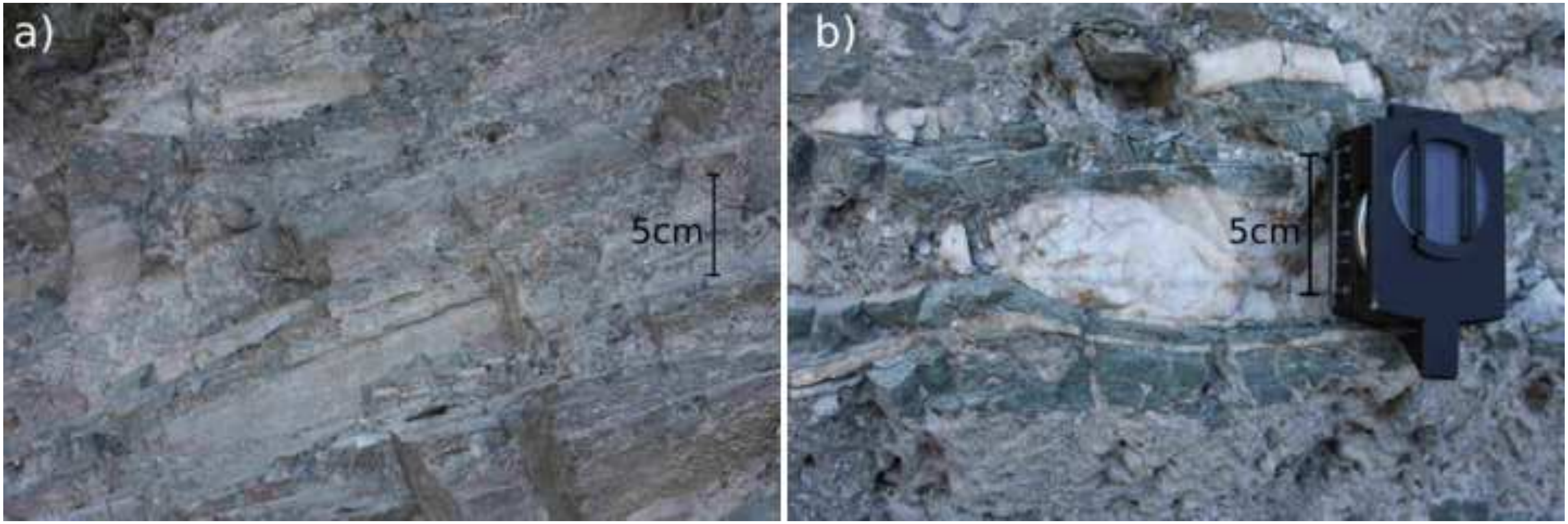
a)
5cm
b)
5cm

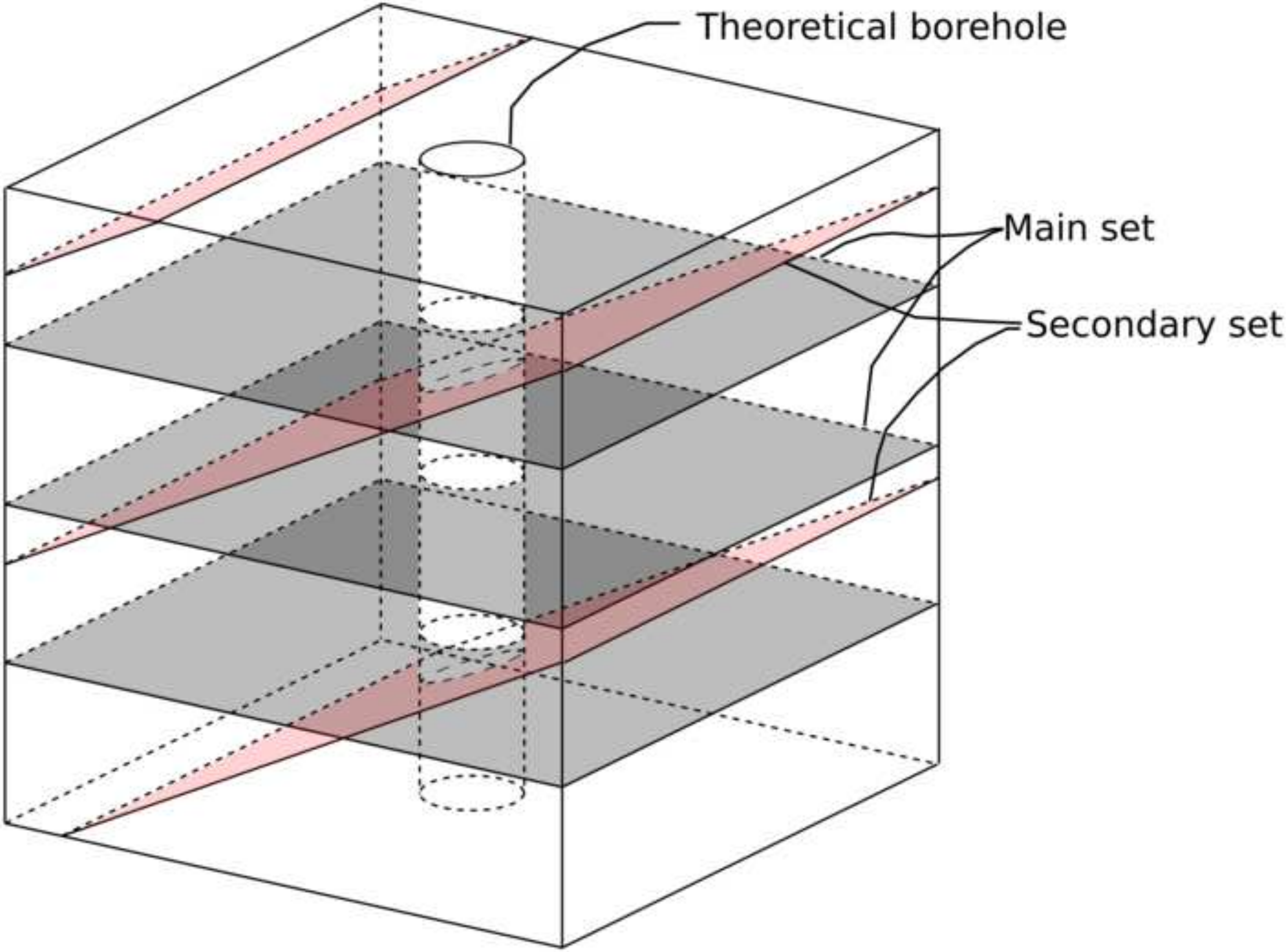
Theoretical borehole
Main set
Secondary set

Figure 5: 129mm 1200dpi. Inkscape

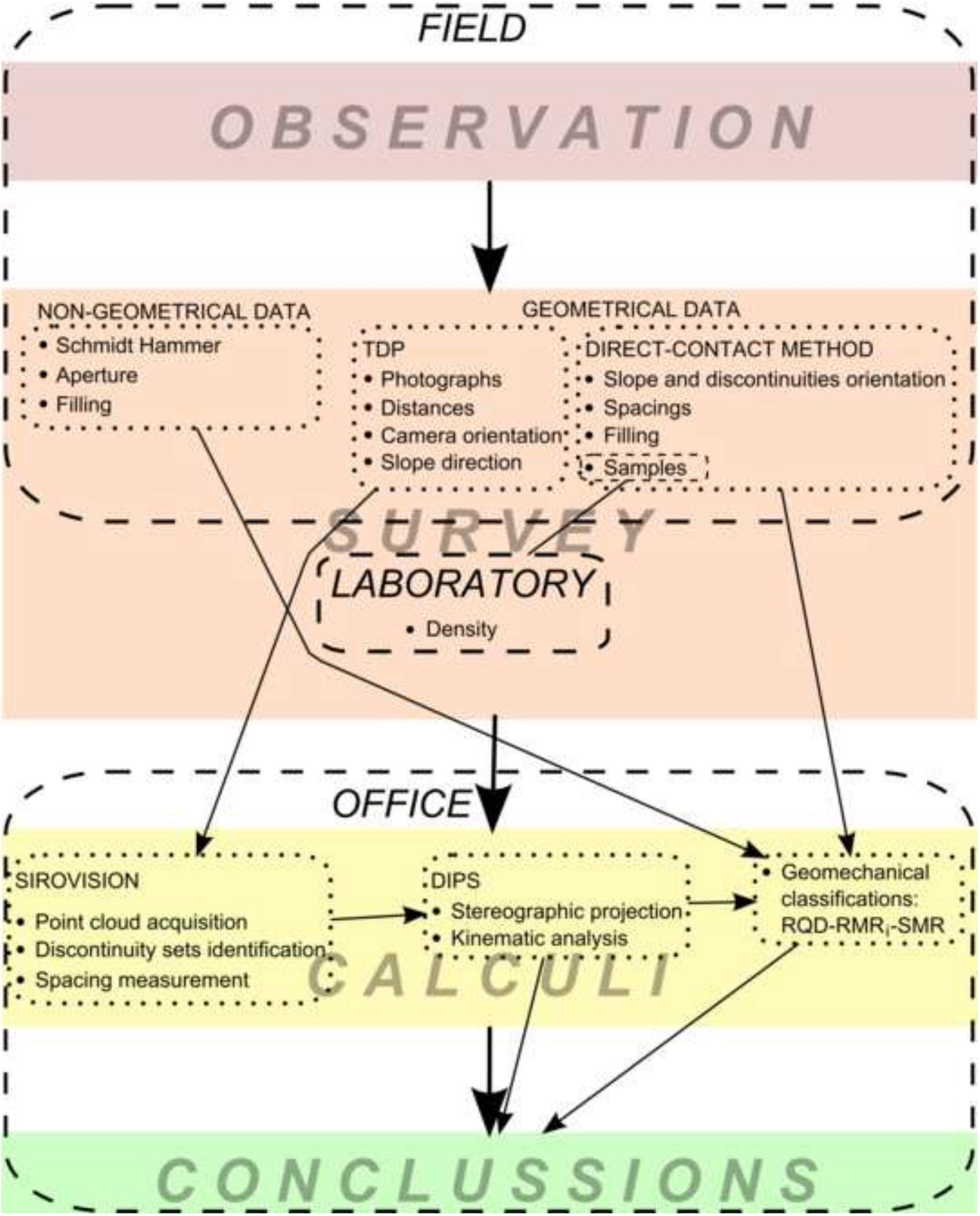

Figure 6: 129mm 850dpi. Inkscape and GIMP,

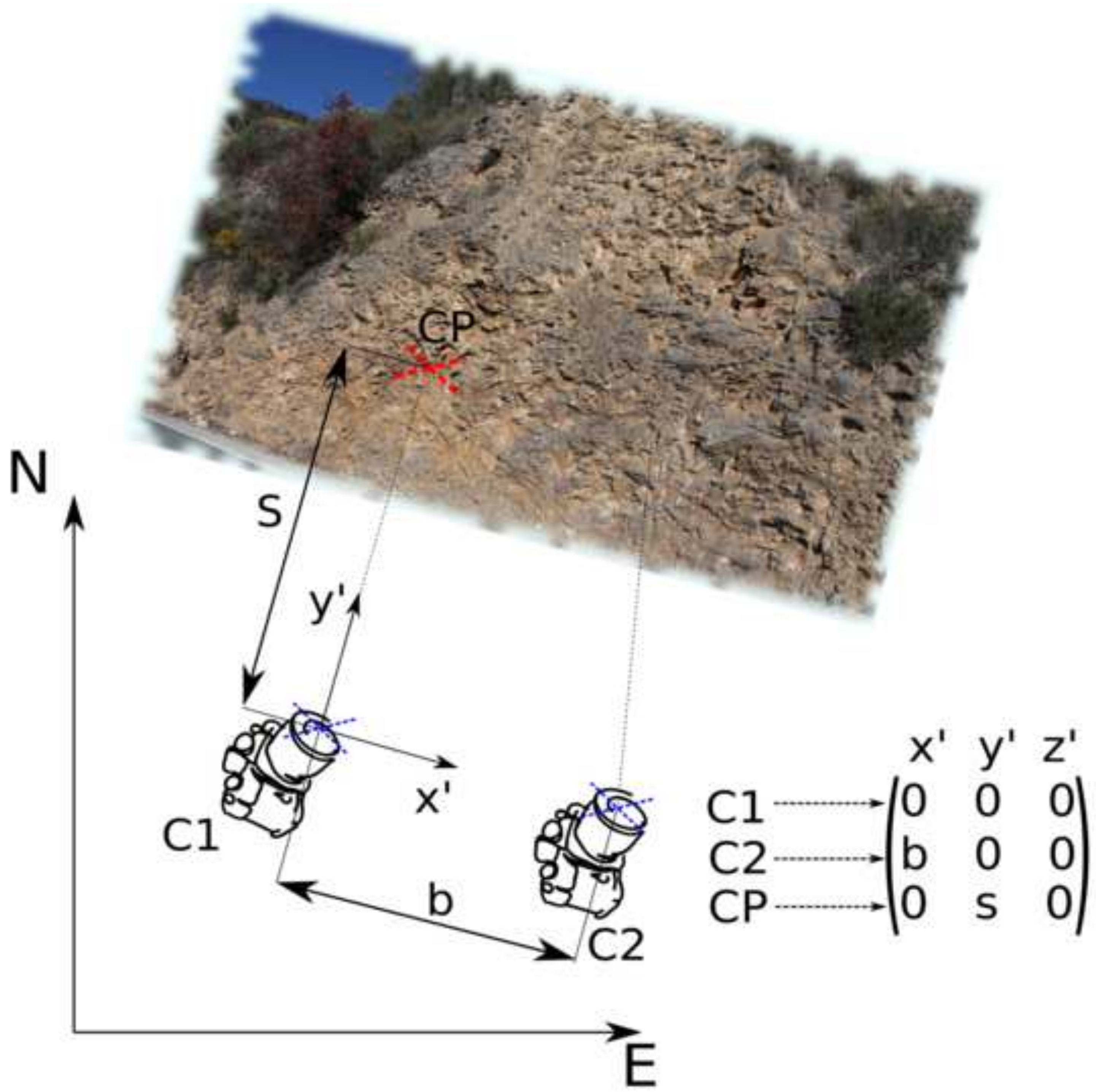

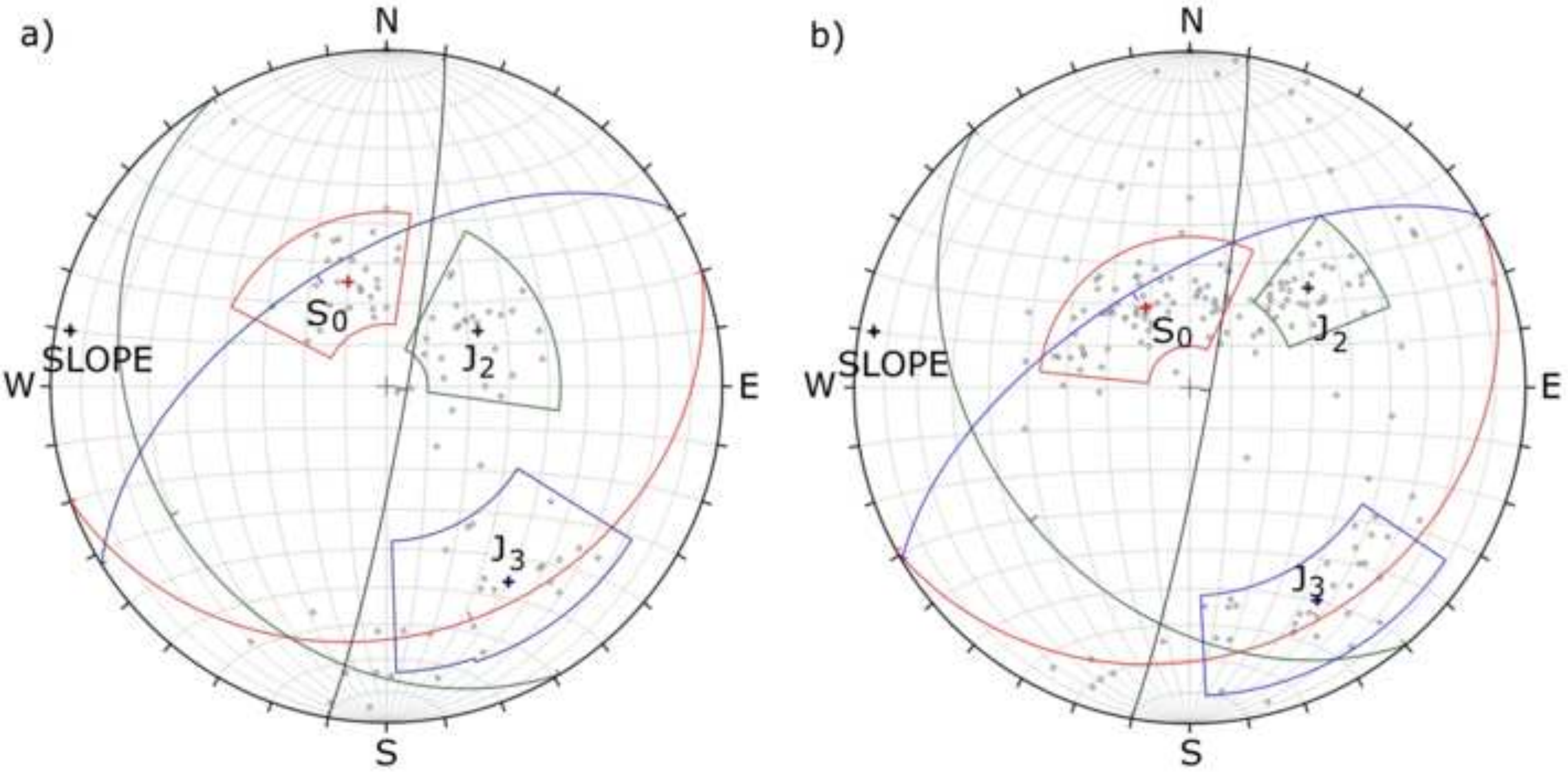
a)
N
E
S
W
SLOPE
S_0
J_2
J_3
b)
N
E
S
W
SLOPE
S_0
J_2
J_3

Figure 8: 174mm 600dpi. Created with DIPS (Rocscience) and modified with GIMP

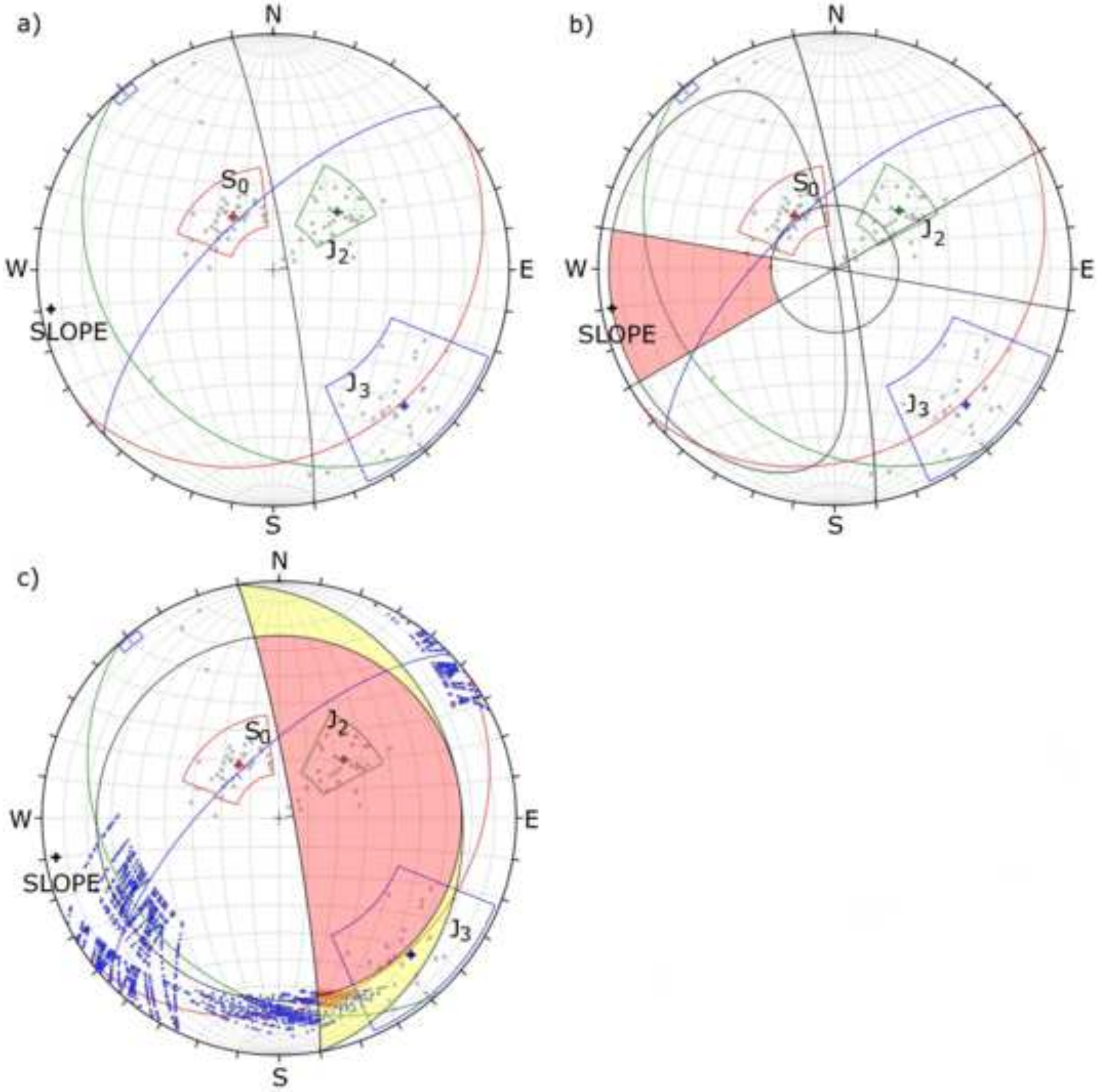

Figure 9: 174mm 600dpi. Created with DIPS (Rocscience) and modified with GIMP

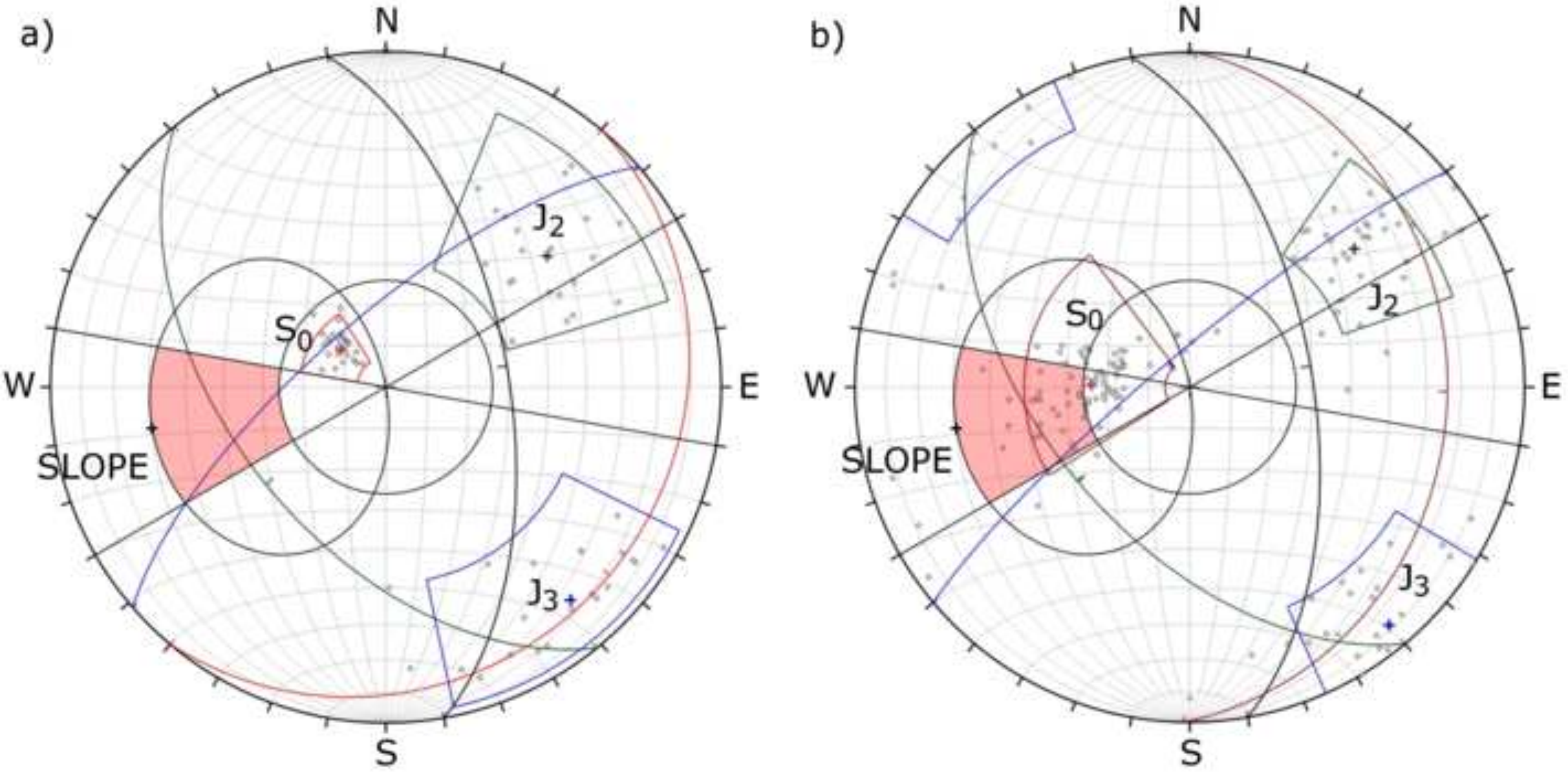

Figure 10: 174mm 1200dpi. Gimp and Inkscape

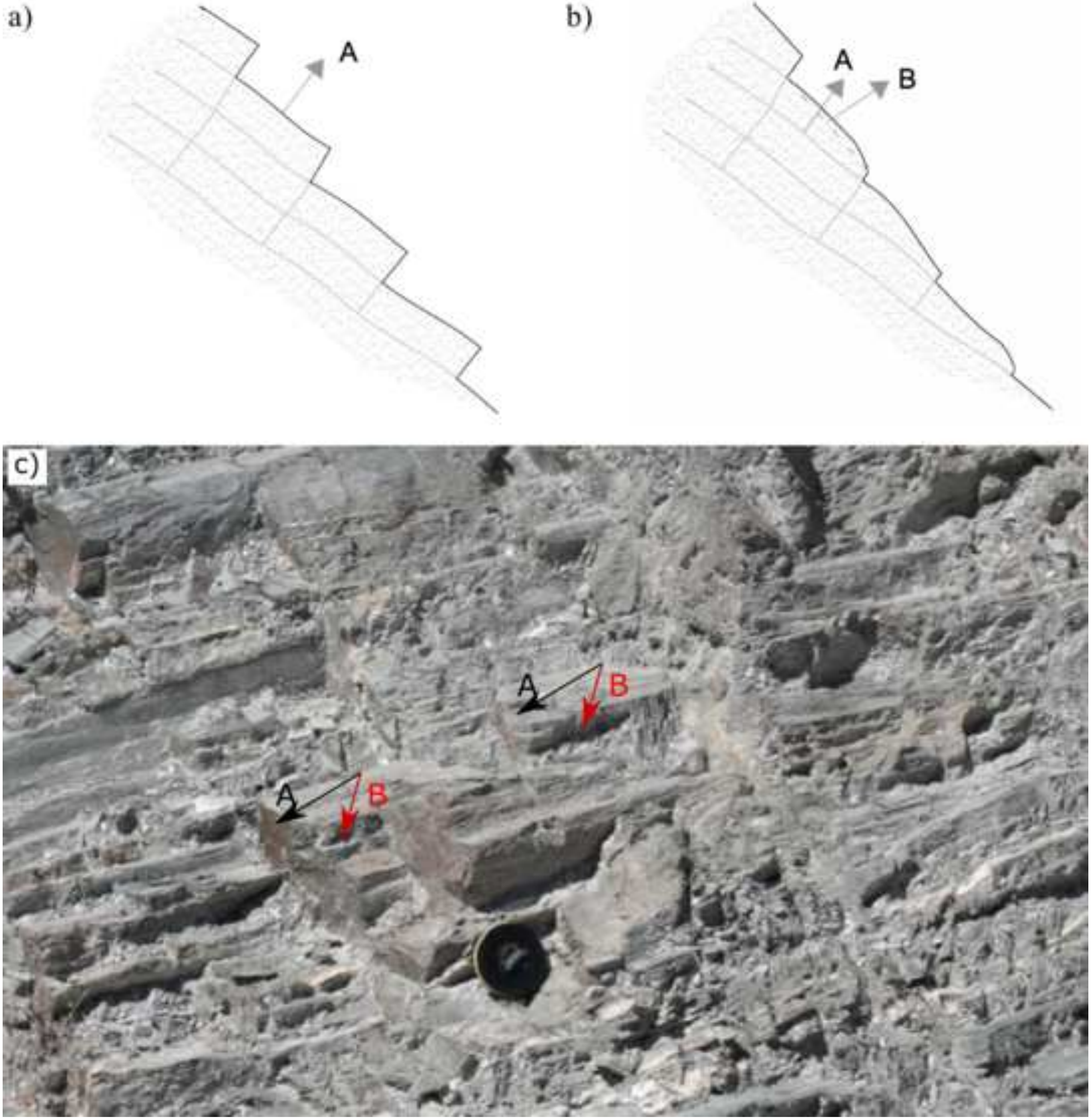

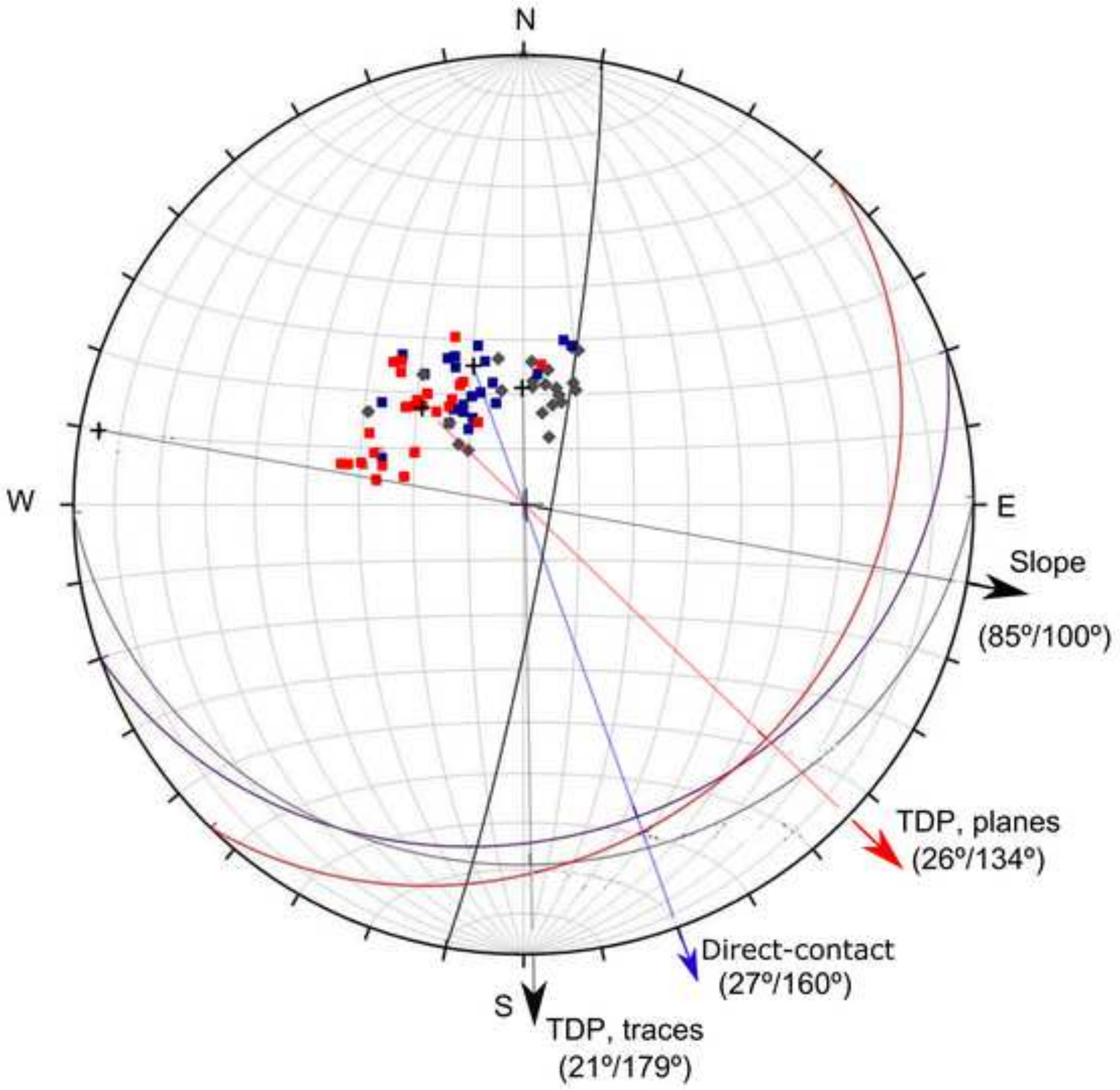
N
W
E
S
Slope
(85º/100º)
TDP, planes
(26º/134º)
Direct-contact
(27º/160º)
TDP, traces
(21º/179º)